

SPACE-TIME STRUCTURE AROUND THE TRANSITION POINT IN CHANNEL FLOW REVEALED BY THE STOCHASTIC DETERMINISM

Hiromu Shimiya

Faculty of Science and Engineering,
Waseda University
3-4-1 Ookubo, Shinjuku-ku, Tokyo, 169-8555, Japan

Ken Naitoh

Faculty of Science and Engineering,
Waseda University
3-4-1 Ookubo, Shinjuku-ku, Tokyo, 169-8555, Japan
k-naito@waseda.jp

ABSTRACT

The transition to turbulence (Reynolds, 1883) has attracted people. Large eddy simulation (LES) and direct numerical simulation (DNS) of the transition to turbulence in straight channels employed the spatial cyclic boundary conditions between the inlet and outlet of the channel. (Moin and Kim, 1982; Kawamura and Kuwahara, 1985) Thus, these previous researches capture only the transition in time, although the spatial transition point where the laminar flow changes to turbulence could not be computed. Recently, some approaches tried to compute the transition point in straight channel for the flows having large disturbances at the inlet. (Oida and Kuwahara, 2003) However, computations of the transition points in the flows with various inlet-disturbances and also for various Reynolds numbers are still in an infant stage, although it is necessary to predict the transition points for airfoil optimizations and micro-fluids such as blood and fuel cell. Thus, we proposed the method called “stochastic determinism”, based on the deterministic Navier-Stokes equation and stochastic artificial disturbances. (Naitoh et al., 2008) Here, we show the method in detail and also clarify the space-time structure after an impulsive start for a wide range of Reynolds numbers.

STOCHASTIC DETERMINISM

Convergence criterion for the matrix calculation in computational fluid dynamics has been based on mathematics until now. (Roache, 1972.) However, the numerical errors should be used adequately on the basis of physical evaluation, because we cannot simulate the unstable asymmetric flows such as Karman vortex streets without numerical disturbances. Asymmetric distribution of numerical errors in space brings the up-and-down asymmetric flows, although people have not mentioned explicitly. We should find the appropriate values of the numerical errors in the analytical domain, which correspond to the physical fluctuations. We propose the physical criterion of convergence, appearing after scales falling from our eyes, in which the level of numerical truncation errors is related to actual velocity fluctuation at the inlet. Combination of this physical criterion and the finite

difference method extended based on the multi-level formulation (Naitoh and Kuwahara, 1992), which can calculate spatial derivatives of physical quantities and integrated quantities accurately, leads us to the new stage of computational fluid dynamics.

Starting point of the methodology is related to the equation of the divergence of velocity in the multi-level formulation, which is transformed from the compressible Navier-Stokes equation while maintaining the Gibbs formula. (Naitoh and Kuwahara, 1992.) The formulation shows that the second derivative of velocity, the divergence of velocity, controls the physical quantities such as pressure, velocity, and temperature. Thus, in the following sections, we will focus on the control of the numerical error of the divergence of velocity.

NUMERICAL METHOD

The three-dimensional incompressible Navier-Stokes equation in non-conservative form is employed as the governing equation (Eq. 1).

$$\vec{F} \equiv \begin{bmatrix} f_A \\ f_B \end{bmatrix} \left[\begin{array}{c} \sum_i \frac{\partial u_i}{\partial x_i} \\ \frac{\partial u_i}{\partial t} + \sum_j u_j \frac{\partial u_i}{\partial x_j} + \frac{1}{\rho} \frac{\partial p}{\partial x_i} - \nu \sum_j \frac{\partial^2 u_i}{\partial x_j^2} \end{array} \right] = 0 \quad (1)$$

where u_i , p , ρ , x_i , and t denote the velocity component for i -direction, pressure, density, Cartesian coordinate, and time, respectively. Explicit turbulence model is not used in the present report. Boundary conditions at the inlet are $u_1 = U_0 + \delta$, $u_2 = 0$, and $\frac{\partial p}{\partial x_1} = 0$, where U_0 and

δ denote the main constant velocity and random disturbance at inlet, while the well-known outlet condition of spatial derivative of all physical quantities along the direction x_1 being zero. (We must give artificially the disturbance δ at the inlet, because all of the atmosphere on

the Earth at the upstream of the channel cannot be solved. Initial velocity distribution is set to be $u_1(t = 0) = U_0$, $u_2(t = 0) = 0$ at each point.

In the present research, the numerical error \mathcal{E} $[= (\sum_n^N \frac{\partial u_i}{\partial x_i} / N) \Delta x]$ is set to be proportional to δ

corresponding to actual inlet-fluctuation of velocity, where N and Δx denote the total number of grids and grid size.

Concrete numerical method is based on the multi-level formulation (Naitoh and Kuwahara, 1992) generalized from the MAC method. (Harlow and Welch, 1965) Magnitude of \mathcal{E} can be controlled by the number of iterations in the SOR method.

In order to get the solutions of higher-order of accuracy, the correlation of velocity based on Eq. (2) is also included.

$$\int_V \sum_i \frac{\partial u_i}{\partial x_i} dS = 0 \quad (2)$$

where V in Eq. (2) denotes the control volume, which can be taken at several sizes from a cell to channel. In the present report, the volume V is that between the inlet surface and each grid surface which is orthogonal to the channel axis. (Naitoh et al, 2008)

Finite-difference scheme with a third-order of accuracy is used for the convection term and also the other terms in space are with second-order central difference, while the Euler scheme of first order and the Runge-Kutta scheme of forth-order of accuracy are tested in time.

Homogeneous and orthogonal grid system with regular grid distribution is used, because each direction should be same for capturing vortices. Grid systems of $2,500 \times 50 \times 50$ points and $5,000 \times 100 \times 100$ points are tested.

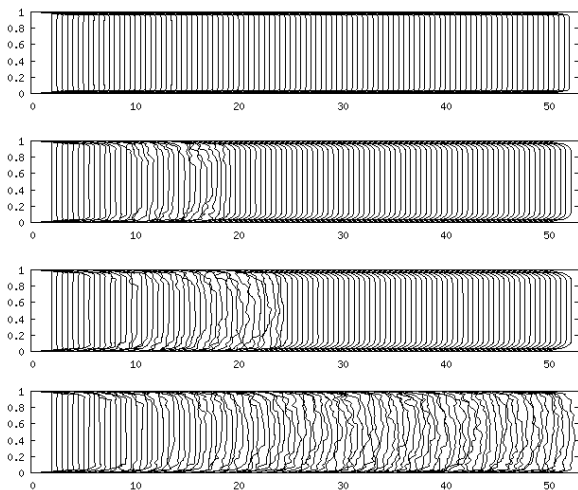


Fig. 1 Instantaneous velocity distributions in the cross-section of $x_3/D=0.5$ and $x_1/D=0 \sim 50$ in a straight channel from initial impulse flow to $t = 100$. (Inlet disturbance is 0.015%. $Re=20,000$. Grid points = $5,000 \times 100 \times 100$. 4th order Runge-Kutta. $(\sum_n^N \frac{\partial u_i}{\partial x_i} / N) \Delta x = \delta$)

RESULTS

Figure 1 shows the instantaneous velocity distributions computed with the inlet-disturbance against the inlet-velocity U_0 of about 0.015% for $Re = 20,000$. We can see that the instability due to strong shear stress in the upstream region brings the transition at the middle part of the channel. Instability cannot start at downstream region, because the thicker boundary layer is in weaker shear stress.

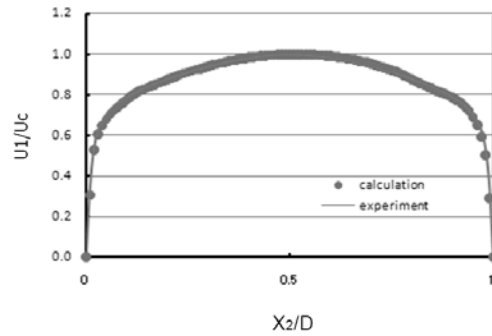
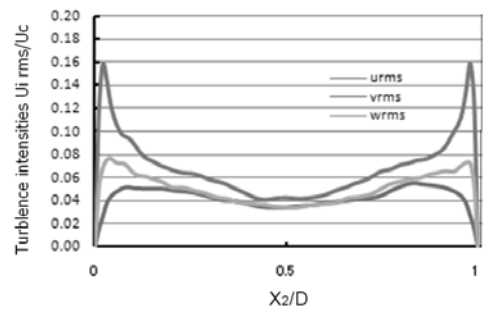
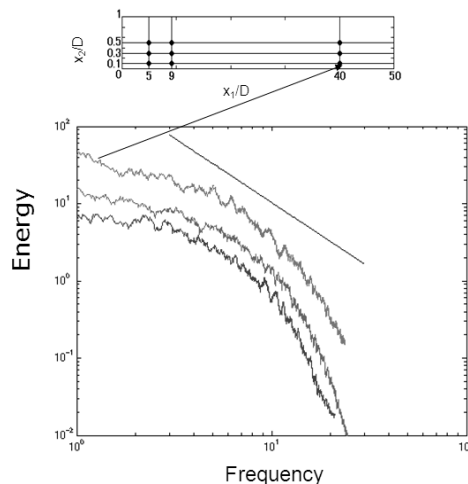


Fig. 2 Time-averaged velocity distribution. (Inlet disturbance is 0.015%. $Re=20,000$. Grid points = $5000 \times 100 \times 100$. The 4th order Runge-Kutta. Experiment by Laufer.)



(a)



(b)

Fig. 3 Turbulence intensities and energy spectrum computed for $t = 50-100$. (a)Turbulence intensities, (b) Energy spectrum: Upper line for $x_2/D=0.1$. Middle line for $x_2/D=0.3$. Lower line for $x_2/D=0.5$. (Inlet disturbance is 0.015%.

Re=20,000. Grid points = 5000×100×100. The 4th order Runge-Kutta.)

Computational mean velocities agree fairly well with the well-known experimental data (Laufer, 1950, Nikuradse, 1932). (See Fig. 2.) The magnitude of turbulence intensity is close to the value well-known (Kawamura and Kuwahara, 1985), while the energy spectrum plotted against frequency also has the gradient of -5/3 partially. (See Fig. 3.)

We examined the influence on the flow of grid size, also by using smaller number of grids of 2,500 x 50 x 50. (See Fig. 4.) Computation with 5,000 x 100 x 100 does not differ from that of 2,500 x 50 x 50 very much.

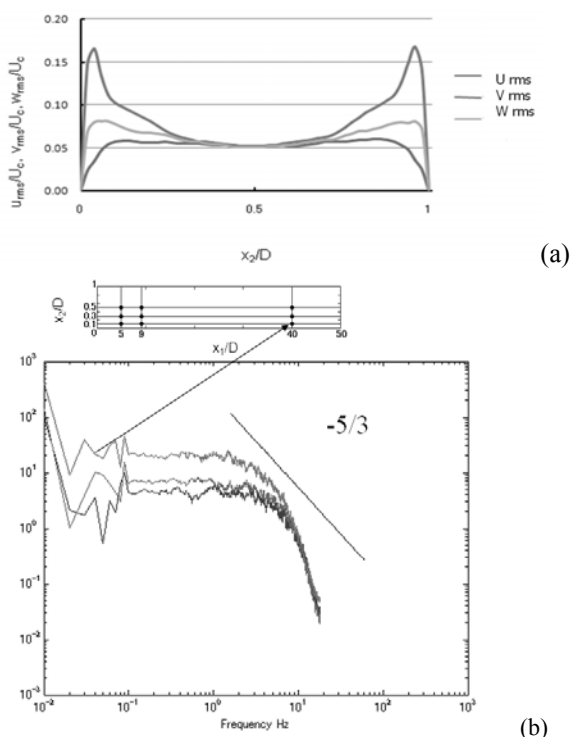


Fig. 4 Turbulence intensities and energy spectrum computed for t=100 – 200. (a) Turbulence intensities, (b) Energy spectrum: Upper line for $x_2/D=0.1$. Middle line for $x_2/D=0.3$. Lower line for $x_2/D=0.5$. (Re=20,000. Grid points = 2500×50×50. 1st order Euler scheme. K.Naitoh et al., 2008)



Fig. 5 Influence of inlet turbulence on the transition point. (Re=20,000. Grid points = 5,000×100×100. 4th-order Runge-Kutta scheme is used. $(\sum_n \frac{\partial u_i}{\partial x_i} / N) \Delta x = \delta$)

Then, computations show that the transition point from laminar to turbulent flow moves according to increasing disturbances at the inlet. (Fig. 5)

Combination of physical evaluations of numerical errors and the numerical method based on the multi-level formulation makes it possible to simulate the transition point in space for various inlet-disturbances.

PHYSICS UNDERLYING THE TRANSITION

Next, we reveal the space-time structure for a wide range of Reynolds numbers.

Figure 6 shows the relation between Reynolds number and the transition point, while the turbulence intensity at the inlet is fixed. Increasing Reynolds number brings earlier transition.

Figure 7 shows the attractor (path of particle) around the transition points computed. An important point is that the early stage of the transition for low Reynolds number of 6,000 shows two-dimensional oscillation, although relatively high Reynolds numbers suddenly bring three-dimensional flow. The present approach may clarify the essential feature underlying the transition to turbulence.

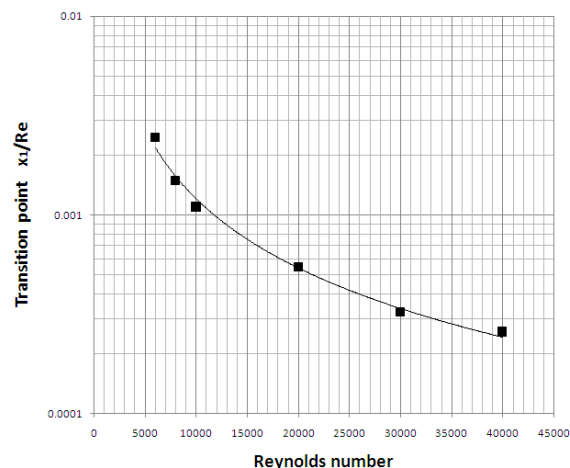


Fig. 6 Relation between Reynolds number and the transition point. (Grid points = 2500×50×50. The 1st order Euler scheme is used.)

FINER SOLUTION OF THE BOUNDARY LAYER

In the previous sections, we employed the grid system based on the Cartesian coordinate, which has a constant size of grid for each direction of three-dimensional space. (See Fig. 8(B).) The homogeneous grid size for each direction will be necessary to resolve the transition to turbulence accurately. Only the aspect ratio of grid of 1.0 [$\Delta x_i / \Delta x_j = 1.0 (i=1-3, j=1-3)$] brings the accurate resolution of turbulence, although most of the previous computational fluid dynamics has used rectangle grid system such as Fig. 8(A) in the boundary layer. The orthogonal grid system based on the Cartesian coordinate should be also used, because non-orthogonal grid systems produce a lot of artificial viscosity unreal.

However, the homogenous and orthogonal grid system also has a weak point, which cannot resolve the boundary layer in detail, because the grid points are distributed homogeneously in the analytical domain. Thus, we propose a new methodology of “cradle grid system”, which can

compute the boundary layer in detail, while maintaining the homogenous and orthogonal grid system.

First, we prepare two grid systems of Figs. 8(B) and (B'), which have same grid size, although the grid system (B') is translated in parallel with the distance of $\delta\xi$. Cradle grid system of Fig. 8(C), i.e., combination of Figs. 8(b) and 8(B'), brings us some more grid points close to the wall in order to analyse the boundary layer, while maintaining homogenous and orthogonal grid system.

We must propose also the numerical algorithm, how to use the new grid system in Fig. 8(C). Alternately in time, we employ the two grid points of Fig. 8(B) and (B'). Then, the mathematical interpolation of Hermit is used for interpolating the physical values between Grid (B) and Grid (B') (See Fig. 9 and Eqs. (3) and (4).)

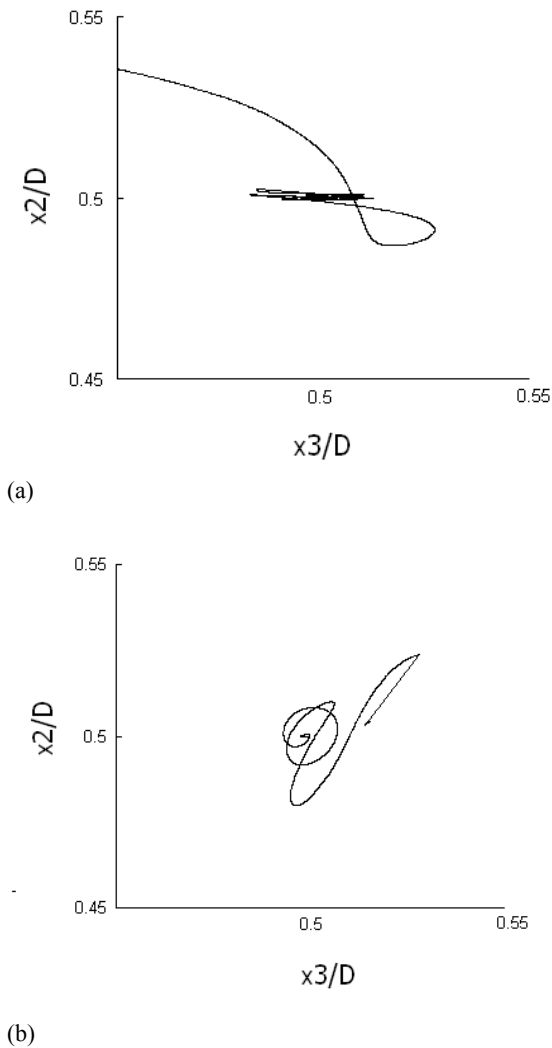


Fig.7 Attractor (path of particle) around the transition point, which is seen from the main flow direction of x_1 . (Grid points = $2,500 \times 50 \times 50$. The 1st order Euler scheme is used.) (a) $Re=6,000$ (b) $Re=20,000$.

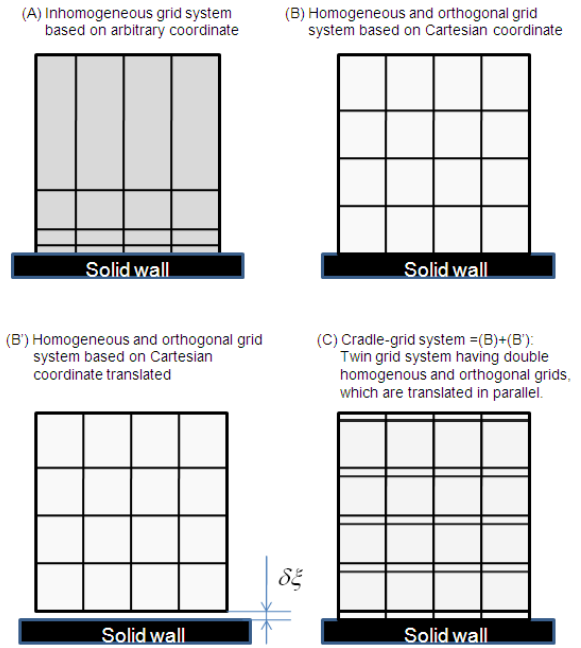


Fig. 8 Cradle grid system.

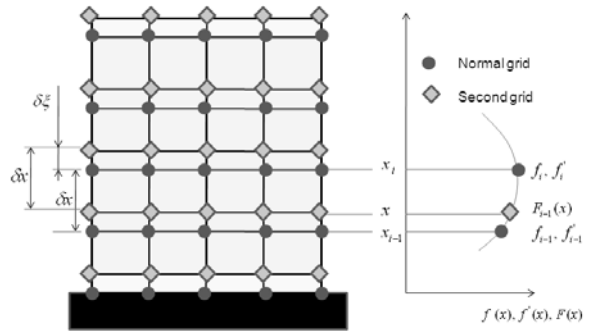


Fig. 9 Computational algorithm on the cradle grid system.

$$F_{i-1}(x) = a_i(x - x_{i-1})^3 + b_i(x - x_{i-1})^2 + f'_{i-1}(x - x_{i-1}) + f_{i-1} \quad x_{i-1} \leq x < x_i \quad (3)$$

$$a_i = \frac{(f'_i + f'_{i-1})\Delta x - 2(f_i - f_{i-1})}{\Delta x^3}$$

$$b_i = \frac{3(f_i - f_{i-1}) - (f'_i + 2f'_{i-1})\Delta x}{\Delta x^2}$$

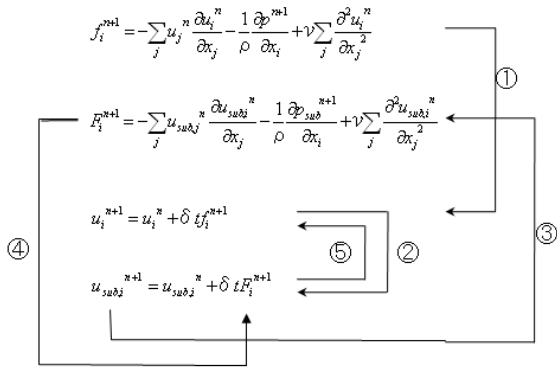
(4)

Careful consideration is necessary for the interpolation. We propose the details for interpolation in Fig. 10. The Hermit interpolation is done only for the terms except for temporal derivatives.

Here, we set to be $\delta\xi = \delta x / 2$. Figure 11 shows the time-averaged velocity distribution computed by using the cradle grid system. We can see more grid points inside the normal

grid system of Fig. 8(B), while the numerical results of mean velocities and turbulence intensities are similar to those on the homogenous and orthogonal grid system on only Fig. 8(B). (See Figs. 11 and 12.)

[This methodology essentially differs from the immersed boundary methods. (Kim, J., Kim, D., and Choi, H., 2001.)]



f : values at the normal grid
 F : values at the second grid

②, ⑤: substitution after Hermit interpolation between f and F

Fig. 10 Five steps of computational algorithm on the cradle grid system.

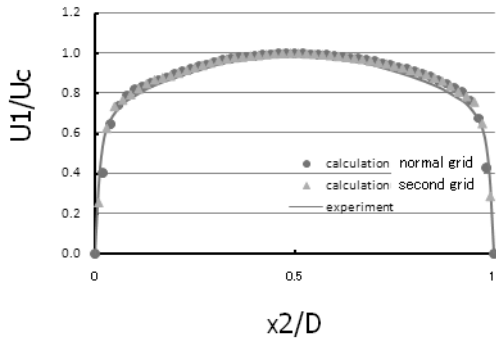


Fig. 11 Time-average velocity distribution due to cradle grid system. (experiment by Laufer.)

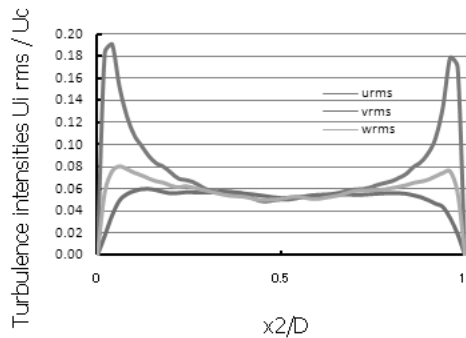


Fig. 12 Turbulence intensities due to the cradle grid system.

VALIDITY OF STOCHASTIC DETERMINISM

In this section, we clarify the reason why the above approach (stochastic determinism) works well.

Fundamentally, fluids such as air are not a continuum because of their discrete molecules. Let us consider the smallest size of vortices, the Kolmogorov scale. This is on the order of 100 – 1000 times as large as the mean free path in high Reynolds number flows. Thus, the molecular discontinuity brings small stochastic value of 0.1 % at most in the Kolmogorov-scale vortex at the edge of continuum assumption. (See Fig. 13.) Moreover, the instability area before the transition may bring a characteristic scale smaller than the Kolmogorov scale. This smaller scale leads to larger stochasticity. Thus, this gap between the phenomenon and continuum mechanics clearly exists and leads to stochasticity. Continuum assumption cannot evaluate the stochasticity. For these reasons, the deterministic models such as the incompressible Navier-Stokes equations based on continuum assumption are essentially defective for solving the transition.

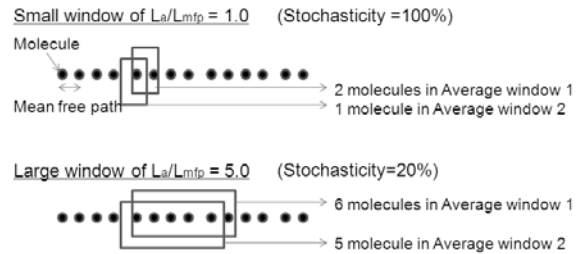


Fig. 13 Stochastic level related to window-size for averaging. If the window-size is close to the mean free path of molecule, the number density varies very much according to the translation of the window. The ratio of mean free path and average window size is equal to the stochastic level. (Stochasticity = Mean free path / Window size)

In order to evaluate the smallest characteristic scale in the instability area before the transition, we use the governing equation averaged in a smaller window (stochastic determinism window) than that for continuum mechanics.

The equation averaged in the stochastic determinism window leads to the divergence of velocity nonvanishing, while the physical quantities such as velocity and pressure averaged in the stochastic determinism window include weak indeterminacy.

Moreover, inlet disturbances and turbulence also lead to small density variations such as a very weak compressibility, i.e., divergence of velocity nonvanishing.

Therefore, mass conservation in these equations can be described by the unified form of

$$\sum_{i=1-3} \frac{\partial u_i}{\partial x_i} = \varepsilon \tag{5}$$

where u_i , x_i and ε denote the quantities of stochastic determinism velocity components for the i -direction, stochastic determinism pressure, Cartesian coordinates, and divergence of velocity, respectively.

One of the reasons why the previous attempts such as those of Moin and Kawamura could not compute the transition point in space is that the criterion of \mathcal{E} in Eq. (5) was set to zero based on mathematics, not on fluid physics taking into account weak compressibility and discontinuity. Evaluations of \mathcal{E} in the previous reports were too small to represent the actual physical fluctuations of velocities. [Increasing inlet-disturbance will reduce the characteristic scale in the instability area, related to the thickness of laminar boundary layer (L.B.L.) and also the inhomogeneous velocity distribution in the layer. Thus, we change of the size of the stochastic determinism window according to the inlet-disturbance.]

CONCLUSIONS

1. Present numerical approach

There are many application problems of the present method, which are blood flows, flows inside fuel cell, and laminar airfoils.

Why could not the previous approaches of computational fluid dynamics simulate the transition point in space? There are four reasons. First, people have used only the mathematical evaluation of numerical errors, which we explain above. Second, the correction method based on the multi-level formulation reduces local concentration of numerical errors. Third, most of people would try to compute the channel flows in the short region of $L/D < 50$. Finally, the third-order upwind scheme famous as the implicit LES (Kuwahara et al, 2005) is relatively tough for a wide range of grid size, although homogenous grid distribution leads to less concentration of grids around solid walls.

The cradle grid system with smaller value of $\delta \xi$ will be able to resolve the boundary layer, while capturing the transition.

2. Stochastic determinism and quantum mechanics

Stochastic determinism window, smaller than that for continuum mechanics, brings us the weak indeterminacy of physical quantities such as velocity and pressure. However, the method with indeterminacy is also useful to analyse the phenomena, as is seen in the quantum mechanics with indeterminacy principle.

In this report, we used $(\sum [\partial u_i / \partial x_i] / N) \Delta x = \delta$. In the future, we should employ the dimensionless form of

$$\left(\sum_n^N \frac{\partial \bar{u}_i}{\partial \bar{x}_i} / N \right) = C_e \bar{\delta}$$

and the dimensionless Navier-Stokes equation with the Reynolds number, where C_e will be between 10^{-2} and 10^2 .

3. Random number generator

In the present report, we controlled the stochastic level by varying the number of iterations for the SOR method. However, we can control the stochastic level also by the other approach having two steps. First is to reduce extremely the numerical errors of the divergence of velocity. After that, we put artificial disturbance made by random number generator into each grid point.

REFERENCES

- Reynolds, O., 1883. "An Experimental Investigation of the Circumstances Which Determine Whether the Motion of Water Shall Be Direct or Sinuous, and of the Law of Resistance in Parallel Channels". *Proceedings of the Royal Society of London*, Vol. 35, pp. 84-99.
- Moin, P. and Kim, J., 1982. "Numerical investigation of turbulent channel flow". *J. Fluid Mech.* 118, pp.341-377.
- Kawamura, K. and Kuwahara, K., 1985. "Direct Simulation of a Turbulent Inner Flow by Finite-Difference Method", *AIAA paper* 85-0376.
- Ooida, J. and Kuwahara, K., Implicit LES of Turbulence Generated by a Lattice, 2003 AIAAPaper2003-4097
- Naitoh, K. and Kuwahara, K., 1992. "Large eddy simulation and direct simulation of compressible turbulence and combusting flows in engines based on the BI-SCALES method", *Fluid Dynamics Research* 10, pp.299-325.
- Naitoh, K., Nakagawa, Y. and Shimiya, H., 2008. "Stochastic determinism approach for simulating the transition points in internal flows with various inlet disturbances". *Proceedings of 5th International Conference on Computational Fluid Dynamics, (ICCFD5) (to be published as Computational Fluid Dynamics 2008, Springer)*.
- Harlow, F.H. and Welch, J.E., 1965. "Numerical calculation of time-dependent viscous incompressible flow of fluid with free surface", *Physics of Fluid*, 8, 12.
- Kim, J., Kim, D., and Choi, H., 2001. "An immersed-boundary finite volume method for simulations of flow in complex geometries", *J. of Computational Physics*, 171, pp. 132-150.
- Naitoh, K., 2007. "Computation of transition to turbulence" *Proceedings of the 2007 Annual Conference on Fluid Dynamics, Japan Society of Fluid Mechanics*.
- Naitoh, K., Takagi, Y., and Kuwahara, K., 1993. "Cycle-resolved computation of compressible turbulence and premixed flame in an engine", *Computers & Fluids*, 22, 4/5, pp.623-648.
- P. J. Roache, 1972. *Computational Fluid Dynamics*, Hermosa.
- Kuwahara, K. et al. 2005. "Development of Implicit Large Eddy Simulation", *Proc. of the 6th Int. Nobeyama Workshop on the New Century of Comp. Fluid Dynamics*, 2003, 47-59.
- Nikradse J, 1932. "Gesetz massigkeiten der turbulenten stromung in glatten rohren." *Forschungs-Arb. Ing-Wesen*, No. 356.
- J.Lauffer, J. 1950. "Investigation of turbulent flow in a two-dimensional channel", *NACA Technical Note* 2123, 68.

ACKNOWLEDGEMENT

The authors express sincere thanks for the help on visualizations of the computational results of Mr. H. Maeguchi of the Naitoh Laboratory, Waseda University. The authors also express sincere thanks for their help on using the super-computer of Osaka University, Cyber media center (<http://www.hpc.cmc.osaka-u.ac.jp/>).